communications earth & environment

Article

A Nature Portfolio journal

https://doi.org/10.1038/s43247-025-02372-4

Fingerprint of anthropogenic climate change detected in long-term western North American fire weather trends

Laura E. Queen[1,2] ✉, Sam Dean[2], Dáithí Stone[2], Piyush Jain[3], James Renwick[1], Nathanael Melia[1,4] & Yukiko Imada[5]

The anthropogenic fingerprint has been detectable in observed global climate change for decades, yet it is still difficult to detect at the regional scale beyond temperature due to the presence of large internal variability and modeling and observational uncertainties. Here we demonstrate regional optimal fingerprinting of long-term fire weather trends in western North America, leveraging large ensembles of high resolution, atmosphere-only climate models to adequately sample internal variability. Considering the full spatiotemporal response to thermodynamic and dynamic climate change, we find that anthropogenic forcings have contributed 81–188% of the region's observed increasing linear trend in fire weather over the last 50+ years. The natural fingerprint, which contains inter-annual and decadal variability, is also robustly detected. We detect the anthropogenic fingerprint in relevant meteorological variables – temperature, precipitation, and relative humidity – and link model differences in fire weather response to differences in simulated precipitation and relative humidity responses.

Wildfires across western North America (WNA) have increased in intensity and frequency over the past half-century[1,2], posing an increased risk to lives and livelihoods. While wildfires are a natural part of many North American ecosystems, various factors could be contributing to these observed trends, including forest management, land-use change, changes to fire ignition[3–5], anthropogenic climate change, and natural climate variability and forcings[6,7]. At a daily time-scale, regional wildfire activity is largely driven by weather conducive to fire ignition and spread – called 'fire weather' – which is categorized by hot, dry and windy conditions. A warming and drying climate has led to regional decreases in fuel moisture, increases in fire weather extremes, fire growth risk and increasing fire season lengths[7–10]. For WNA, where many of these changes have a robust trend, a clear relationship between increasing fire weather and area burned has been established[11–15].

The task of attributing these observed changes to anthropogenic climate change has largely been done through the lens of 'extreme event attribution', which examines whether and to what extent the probability of a particular extreme event has changed due to anthropogenic climate change[16]. Increasingly applied to climate impacts across the world, such as heatwaves and flooding, event attribution methods have recently been used to study extreme fire events and seasons in Australia[17,18], Europe[19,20], and North America[21–26]. In the WNA region, these studies have shown that anthropogenic climate change made the fire weather conducive to the 2016 Fort McMurray fires in Canada 1.5–6 times more likely[24], the extreme fire weather conducive to autumn wind-driven fires in northern California and Oregon 1.4 times more likely[23], and the fire weather underlying the extreme 2017 fire season in British Columbia 2–4 times more likely[25]. At the global scale, probabilistic approaches have attributed shifts in extreme fire weather distributions to anthropogenic versus natural factors[27] as well as individual anthropogenic factors, e.g. greenhouse gas versus aerosol emissions[28].

Few studies have assessed how natural and anthropogenic factors may be contributing to long-term observed fire weather trends. Those that do use various approaches which make assumptions to increase signal to noise, including the assumption that changes to fire weather are spatially uniform[29,30] or unaffected by anthropogenic circulation and precipitation changes[11,29,31]. The foremost attribution study of long-term fire weather trends, Abatzoglou and Williams (2016)[11], remove the anthropogenic signal, estimated as the low-pass filtered trend of temperature and vapor pressure across a multi-model ensemble, to construct naturalized fire weather time series. Anthropogenic influences on precipitation and circulation were not considered due to (1) the assumption that observed changes are entirely due to natural variability, and (2) modelling limitations, as the models used in the study were unable to simulate consistent precipitation and circulation

[1]Victoria University of Wellington, Wellington, New Zealand. [2]National Institute of Water and Atmospheric Research, Wellington, New Zealand. [3]Northern Forestry Centre, Canadian Forest Service, Natural Resources Canada, Edmonton, AB, Canada. [4]Climate Prescience Limited, Rotorua, New Zealand. [5]Meteorological Research Institute, Tsukuba, Japan. ✉e-mail: lauraqueen411@gmail.com

responses. While changes in precipitation extremes across North America have been attributed to anthropogenic climate change[32], the detection and attribution of mean precipitation changes remains an open question due to observational and modelling uncertainties and increased variability at the regional scale[33,34]. Even with adequate modelling of regional circulation responses, the method of constructing naturalized time series by removing model-simulated signals may be appropriate for temperature, but not non-linear circulation responses and their impacts on fire weather. The inherent limitation of this methodology is that the models used do not explicitly simulate the response to anthropogenic and natural climate forcings and variability[20]. As fire weather indices integrate multiple meteorological variables, the attribution of fire weather trends is a complex multivariate problem which depends on the sensitivity to each input variable and their individual, non-linear response patterns[35,36].

In this study, we compare fire weather observations against model-simulated response patterns, assessing fire-climate attribution through the lens of climate change Detection and Attribution (D&A). D&A is the formal process of detecting significant changes in the Earth system and decomposing these changes into distinct natural and anthropogenic 'fingerprints'. Using the established linear regression-based D&A method, optimal fingerprinting, we regress the model-simulated response patterns against observations to determine the relative contribution of natural and anthropogenic factors to the observed patterns. The regression is performed in the direction of maximum signal-to-noise as determined by a decomposition of internal variability. This allows us to assess D&A without reducing the complexity of the problem by either taking large spatial or temporal averages or removing aspects of the climate system, such as the circulation response. Advantages of this approach include (1) simulating the response to both anthropogenic thermodynamic and circulation changes, and (2) considering spatial patterns of change in addition to temporal patterns when distinguishing between anthropogenic and natural fingerprints. We use the Canadian Fire Weather Index (FWI)[37] to examine long-term patterns in observed and simulated fire weather. Originally developed for Canadian forests, FWI estimates potential fire intensity using a combination of meteorological variables - temperature, precipitation, wind and relative humidity - and has been used extensively to study the relationship between climate and fire weather across the world[10,18,20,22,23,38–40].

For decades, optimal fingerprinting[41,42] has been the predominant D&A method used to detect global change, from temperature[43–47], precipitation[48,49], and water vapor[50], to ocean temperatures[51] and streamflow[52]. While regional changes in temperature have become increasingly detectable in the last decade[53–58], regional D&A of precipitation and other climate variables is yet to be a tractable problem due to large internal variability relative to forced signals and increased uncertainty around regional modeling and observational datasets at this scale[33,55,59]. In general, the more complex the fingerprint (i.e., across mountainous regions, looking at multivariate processes), the larger the sampling of internal variability (from long control runs or initial-condition ensembles) is needed[33,60–62].

Considering these documented challenges, we impose strict criteria in the selection of models for this study, including (1) high resolution to capture relevant physical processes and spatial structure (< 100 km), (2) large ensembles of simulations to adequately sample internal variability (> 20), (3) long simulations (> 50 years), and (4) output of FWI input variables at the required temporal scale. Across all D&A modeling archives, including DAMIP and C20C + , only two models satisfy these criteria – d4PDF-G and CAM5. This means, in contrast to most optimal fingerprinting studies[44,47,49,52,53,63–66], we use atmosphere-only models instead of fully coupled climate models to simulate response patterns. Atmosphere-only models are prescribed oceanic boundary conditions in place of a free-running ocean model which removes regional biases in mean sea surface temperatures (SSTs)[67], may improve the simulation of regional circulation patterns[68], removes ocean variability from the noise, and frees up computational space to simulate global, high resolution, large ensembles. The main caveat when using atmosphere-only models is the introduction of the central assumption that anthropogenic climate change is not affecting natural ocean variability. Unlike a simulated ocean response in a coupled model, the prescribed naturalized oceanic boundary conditions are simply detrended observations. If, for example, climate change is altering the variability of the El Niño-Southern Oscillation (ENSO), this anthropogenic factor would be imbedded in the natural simulations. While a disputed issue, there is no robust evidence that climate change has affected natural ocean variability on the time scale of this study (~ 50 years)[69,70].

Results

Modelled fire weather trends

We calculate FWI for two atmosphere-only models, d4PDF-G[71] and CAM5[72], and compare the simulated response patterns against FWI calculated from the European Centre for Medium range Weather Forecast Reanalysis Version 5 (ERA5)[73]. The models simulate all-forcing historic (ALL) and natural-forcing (NAT) counterfactual simulations using prescribed observed and naturalized sea surface temperatures (SSTs) and radiative forcings. We calculate FWI across the large initial-condition ensembles for each model – 100 ALL and NAT members at ~60 km resolution for d4PDF-G and 43 ALL and 49 NAT members at ~100 km resolution for CAM5. The anthropogenic-forcings scenario (ANT) is constructed by subtracting NAT from ALL. As the use of pre-1979 ERA5 output to estimate FWI is not documented, we perform station-based validation to ensure that ERA5-based FWI estimates are reasonable prior to the incorporation of satellite measurements in 1979 (Supplementary Note 1).

To compare FWI behavior estimated from the models versus ERA5, we plot maps of local means and trends across the region (Fig. 1) as well as the grid cell area weighted regional average time series and temporal variance (Fig. 2) for each data source. Results are shown for the ALL scenario May–October mean FWI for the overlapping time windows between ERA5 and the models, 1951–2021 for d4PDF-G and 1959–2014 for CAM5. Each data source is masked based on ERA5 high and low leaf area indices, ensuring only areas with sufficient burnable biomass are included. See Methods for details. Ensemble means for each model are banded by the 5–95th percentiles across the ensemble (Fig. 2a), and the distributions of temporal variance across the ensembles are plotted against the variance of ERA5's regional time series (Fig. 2b).

FWI means and trends across ERA5 and the models share spatial structure which appears to include both latitudinal and orographic influence. CAM5 is hotter and windier than ERA5, while d4PDF-G is cooler (Supplementary Fig 3, 4). As such, d4PDF-G FWI magnitudes are biased low compared to ERA5, particularly in the northern region, while CAM5 magnitudes are biased high across most of the study area. ERA5 trends are larger than trends in both models, particularly d4PDF-G, and trends are greater over 1959–2014 than 1951–2021 (Fig. 1g versus Fig. 1c). This may be in part due to the decadal variability highlighted in Fig. 2, which shows ERA5 FWI values decreasing into the 1980s before increasing into the current decade, making a linear trend analysis sensitive to endpoint selection. While this decadal pattern is strongest in ERA5, CAM5, and to a lesser extent d4PDF-G, replicate it as well. Overall, ERA5 FWI is more variable than what is sampled across the model ensembles (Fig. 2b).

Scaling factors

Using optimal fingerprinting, we compare the model-simulated May–October mean FWI ANT and NAT response patterns against ERA5 FWI, estimating the relative contribution of each scenario to the observed patterns. The comparison is a linear regression which combines the response patterns and determines the scaling factors (regression coefficients) which result in the best reconstruction of the observations. The scaling factors, combined with the response patterns, can be used to estimate the relative contributions of each scenario to the observed patterns. The regression is performed in an empirical orthogonal function (EOF) space based on the decomposition of internal variability which maximizes the signal to noise. Considering the full spatiotemporal signals in this EOF

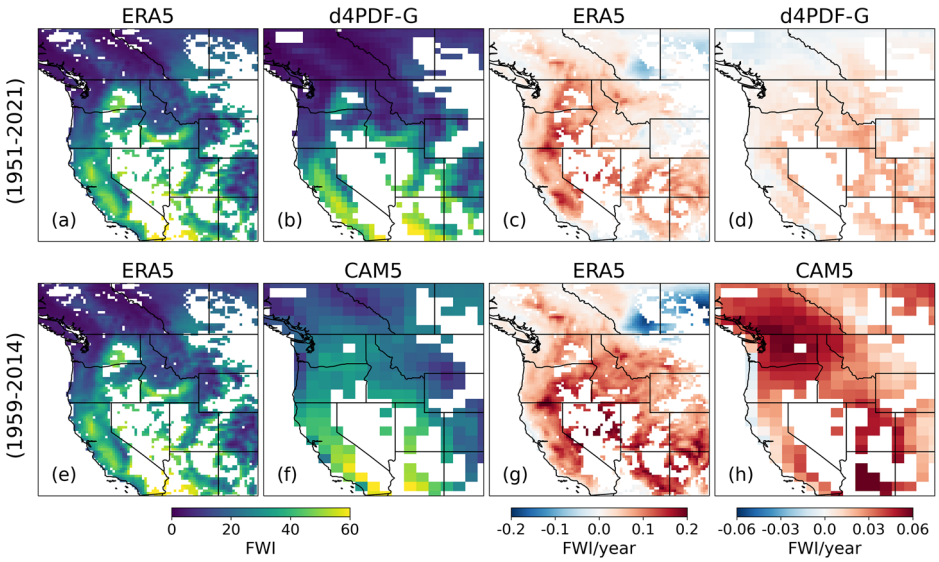

Fig. 1 | Model vs ERA5 FWI climatologies and trends. Mean (**a**, **b**, **e**, **f**) and trend (**c**, **d**, **g**, **h**) maps of May–October mean FWI comparing ERA5 and d4PDF-G (1951–2021; **top row**) and ERA5 and CAM5 (1959–2014; **bottom row**). Trends are the least-square linear regression slope of the time series. Maps are masked by vegetation based on combined ERA5 high and low leaf area indices and plotted in each data source's native resolution.

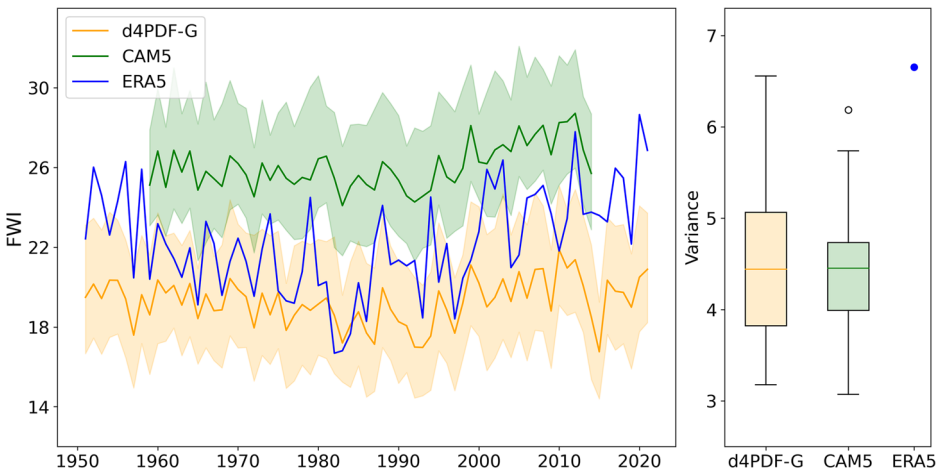

Fig. 2 | Regionally-averaged FWI time series and variance. Vegetation-masked area weighted regionally averaged time series of May–October mean FWI for ERA5, d4PDF-G and CAM5, with the 5–95th percentile range across the ensemble shaded for each model (**left**). Temporal variance of the regional time series for ERA5 (blue dot) and across the ensemble for each model (box and whisker plots) (**right**). The boxes extend from the first to third quartile of variance across the ensemble; whiskers extend from the farthest data point lying within 1.5x the inter-quartile range from the box; outliers beyond the whiskers are plotted as empty circles.

space, the variability unique to each scenario (the fingerprint) is isolated and used to estimate the scaling factors for each response pattern. This EOF space can contain the maximum number of directions of variability, or can be truncated to exclude some directions of variability. The truncation value, which indicates how many EOFs are used, is a subjective choice which can have a significant effect on the results[41,74]. We test optimal fingerprinting across all possible truncations to assess the robustness of the results.

Scaling factors results for each model are shown in Fig. 3, with ANT (red) and NAT (blue) scaling factor best estimates and 90% confidence intervals plotted for the optimal fingerprinting regressions across the full range of truncation levels. Truncation ranges are constrained by the individual ensemble sizes from each model. A fingerprint is deemed as detected if the scaling factor confidence interval does not encompass 0, interpreted as meaning the fingerprint is needed to reproduce the observations. A scaling factor above 1 indicates the response pattern must be amplified to reproduce the observations, while a scaling factor below 1 indicates the pattern must be dampened.

The anthropogenic and natural fingerprints are highly (small confidence intervals) and consistently (across all truncation levels) detectable in both models. For d4PDF-G, the ANT and NAT scaling factors stabilize around 1.5 and 0.7 respectively, indicating the anthropogenic response pattern must be amplified by 50% and the natural response pattern dampened by 30% to linearly combine to best reproduce the observations. In CAM5, both fingerprints must be amplified, ANT by a factor of ~2 and NAT by just above 1, to best combine to reproduce the observed spatiotemporal trends. Qualitatively, these results hold even if the noise is amplified according to the discrepancies between the models and ERA5 variability seen in Fig. 2. As the NAT fingerprint contains SST-prescribed interannual oceanic variability, it is easier to detect (the confidence intervals are smaller) than the anthropogenic fingerprint.

Anthropogenic and natural signals

All data in space and time is used in the fingerprinting regressions – i.e., we do not reduce the dimensions of the signals (the ensemble mean response patterns) or the noise through regional or temporal averaging or linear trend regression. To contextualize the detection and visualize the signals, however, we plot linear trend maps and sub-regionally averaged time series and assess for (in)consistencies between the models.

Least-square regression trends of the FWI ALL and NAT signals are shown for d4PDF-G (1951–2021; Fig. 4a, b) and CAM5 (1959–2014; Fig. 4d, e), alongside their mean noise maps (Fig. 4c, f). Noise across an ensemble is the difference between each ensemble member and the ensemble mean. The 'mean noise' is the average across the ALL and NAT noise ensembles. Regionally averaged time series of the ANT (Fig. 5a, c, e, g) and NAT (Fig. 5b, d, f, h) signals are shown for four sub-regions – Southwest (SW) Canada, Northwest (NW) USA, California, and the Four Corner states (Utah, Colorado, New Mexico, and Arizona). To compare the temporal structure of the signals between the models regardless of magnitude

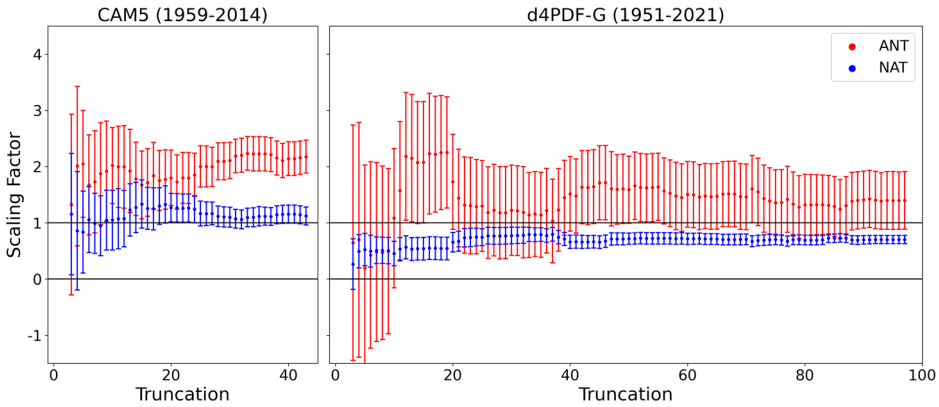

Fig. 3 | Fingerprinting regression scaling factors. Scaling factors and 90% confidence intervals for the anthropogenic (ANT) and natural (NAT) fingerprints for May-October FWI means from each model, d4PDF-G (1951–2021; **right**) and CAM5 (1959–2014; **left**). Scaling factors are estimated from regressions performed in truncated EOF space considering all possible truncation values (the number of EOFs retained). The range of truncation values are constrained by ensemble size: 3–43 for CAM5 and 3–97 for d4PDF-G.

differences, we find the anomaly of each subregional time series by removing the time series mean.

Both models share similar spatial structure in the noise (Fig. 4c, f), with the Four Corner states and eastern Canadian portion of the study area having the largest variability. d4PDF-G also has high variability in northern California and particularly low variability in western Washington and British Columbia. The linear trends of the d4PDF-G signals follow a north/south gradient, with larger ANT increases and NAT decreases in the southern portion of the study area. CAM5 ANT linear trends appear to have more coastal and orographic influence, with trends increasing away from the coast and west of the Rocky Mountains, and the largest increases centering in eastern Oregon, Washington, and western Idaho. CAM5 NAT decreasing linear trends are concentrated in Northern California and Idaho.

The ANT signal contains largely linear trends throughout the study area with minimal decadal variability (Fig. 5a, c, e, g). Both models depict a robust ANT signal in the southern subregions, California (Fig. 5e) and the Four Corners states (Fig. 5g), but deviate in the ANT response in the northern subregions, and particularly the northwestern portion of the study area (Fig. 4a, d). While d4PDF-G shows a slight increasing trend in NW USA (Fig. 5c) and no trend in Canada (Fig. 5a), CAM5 shows robust increases, though the anthropogenic signal appears to emerge later in the northern areas, around the late 1980s in NW USA (Fig. 5c) and the late 1990s in Canada (Fig. 5a).

The NAT signal, however, is dominated by interannual and decadal variability in California (Fig. 5f) and the Four Corners (Fig. 5h) in both models, with the decadal pattern suggesting that linear trend results would be strongly influenced by time-window selection. The NW USA subregion, however, does appear to have linear decreases in NAT FWI in both models (Fig. 5d), while NAT FWI changes in Canada are relatively small (Fig. 5b). These comparisons between the spatial structure of the modelled response patterns and noise are consistent when considering trends over the maximum shared time window, 1959–2014 (Supplementary Fig 11).

As a way of further summarizing the relative anthropogenic versus natural contributions to observed linear trends over the entire domain, we scale the linear trends in the modelled response patterns (Fig. 4a, b, d, e) by the best estimate scaling factor and divide by the observed trends, followed by an grid cell area weighted spatial average. We use the scaling factor estimates from the optimal fingerprinting regression at a truncation level that we find to be representative for a broad range of truncations – 60 for d4PDF-G and 30 for CAM5. About 78% of the variance in the internal variability 'noise' is explained at the chosen truncation value of 60 for d4PDF-G, and about 82% is explained at a truncation of 30 for CAM5. Table 1 shows the estimated contributions from d4PDF-G considering three time windows: 1951–2021 (all available years), 1959–2014 (shared time-window with CAM5), and 1984–2014 (a commonly used period in the literature). Results for CAM5 are shown considering the 1959–2014 and 1984–2014 periods. Contributions are calculated with the best and lower and upper 90th confidence interval scaling factor estimates.

Over the maximum shared time window between the models, 1959–2014, the relative contribution of anthropogenic forcings to the observed linear increases in May-October FWI across the region is between ~81 and 188% as estimated by both models. The anthropogenic contribution counteracts an overall decreasing contribution from the natural response of between −31 and −13% over this period. Over the 1951–2021 time window, d4PDF-G results indicate an anthropogenic contribution of 103% and a natural contribution of −33%. Finally, over the commonly used post-1984 period, results from both models for 1984–2014 estimate 16–88% anthropogenic and 11–26% natural contributions. It is worth reinforcing that natural signals in fire weather were found to be highly detectable but are not well represented by linear trends.

Detectability of meteorological inputs

To assess the robustness of the anthropogenic signal in the underlying meteorological variables contributing to fire weather, we perform optimal fingerprinting on long-term trends of May–October means for each of the FWI inputs (temperature, precipitation, relative humidity and wind) taken from the models, with ERA5 used as the observations. Scaling factor results are shown for a single optimal fingerprinting regression at a truncation level that we find to be representative for a broad range of truncations – 60 for d4PDF-G (Fig. 6a, e, i, m), and 30 for CAM5 (Fig. 6c, g, k, o). Alongside the scaling factor results, we show the ANT signal least-square linear regression trends for 1951–2021 in d4PDF-G (Fig. 6b, f, j, n) and 1959–2014 in CAM5 (Fig. 6d, h, l, p).

The anthropogenic fingerprint is detected (statistically different than 0) for temperature, precipitation, and relative humidity using both models. For temperature, the d4PDF-G ANT signal is not scaled (scaling factor ~1; Fig. 6a), while the CAM5 ANT signal is dampened (scaling factor ~0.6; Fig. 6c) in order to linearly combine with their respective NAT signals to best reproduce the observed trends. The ANT signal for precipitation and relative humidity must be amplified in both models to best reproduce the observations. For d4PDF-G, precipitation must be scaled by ~1.6 and relative humidity by ~1.9, while CAM5 precipitation and relative humidity signals are scaled by ~2.7 and ~1.6 respectively. Wind scaling factor results indicate robust anthropogenic fingerprints could not be estimated from the ANT signals relative to noise, as the response patterns must be amplified by > 6 (Fig. 6o, outside axis limits) or flipped in sign with a factor <−2 (Fig. 6m, outside axis limits) to reproduce the observations.

Spatial structure of the ANT linear trends for each variable are consistent with the FWI ANT trends for each model, with d4PDF-G trends following a north/south gradient (Fig. 6b, f, j, n), and CAM5 trends highlighting coastal and orographic effects of the Rocky Mountains (Fig. 6d, h, l, p). The main divergence between the models is the precipitation and relative humidity anthropogenic response in the northwest portion of the study area, where d4PDF shows increasing precipitation and relative humidity trends and CAM5 shows decreasing trends for both variables.

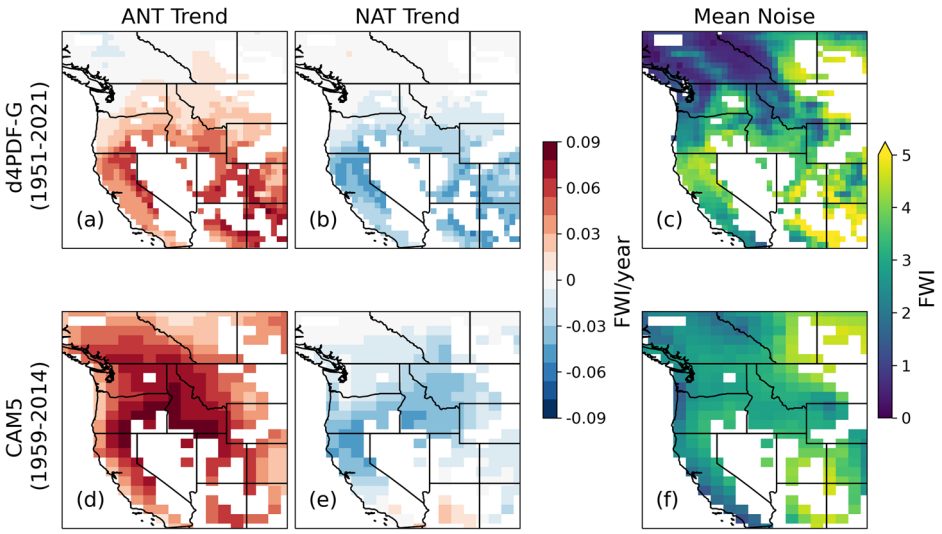

Fig. 4 | Model-simulated signal trends and noise. Trend maps of the ensemble mean anthropogenic (**a**, **d**) and natural (**b**, **e**) signal trends (least-square regression slope) of May–October mean FWI for d4PDF-G (1951–2021; **top row**) and CAM5 (1959–2014; **bottom row**), as well as the mean noise maps (**c**, **f**). Noise across an ensemble is the average absolute deviation from the ensemble mean for each ensemble member; mean noise is the average across both ALL and NAT noise ensembles.

Discussion

Using optimal fingerprinting with global, atmosphere-only models, we detect a robust anthropogenic fingerprint in long-term fire weather across WNA – i.e., the observed spatiotemporal FWI trends could not be reproduced without the contribution of the anthropogenic fingerprint. Both models simulate robust anthropogenic signals in the southern portion of the study area, with California having consistently large signals alongside relatively low variability. Anthropogenic signals in the northern areas are less certain, consistent with the late emergence of a climate signal in the observed records in British Columbia[75]. The natural fingerprint, which contains SST-prescribed natural oceanic variability like ENSO, is also easily detectable in the observations.

As our study uses model simulated response patterns to anthropogenic and natural factors, we capture non-linear circulation and thermodynamic driven changes in each meteorological variable and the impact of these changes on fire weather. This improves upon previous fire D&A studies which reduce the complexity of the problem by simply detrending the meteorological inputs to construct a counterfactual time series[11,20], and/or relying on the assumption that changes to fire weather are spatially uniform or due to anthropogenic changes in temperature and relative humidity alone[11,29,31]. Justifications for excluding anthropogenic circulation and precipitation changes from previous studies include the assumption that these changes are due to natural variability alone, as well as the limitations of climate models to consistently simulate regional circulation and precipitation responses. Here, however, we show that the anthropogenic fingerprint is detectable in observed 6-month mean precipitation changes using both atmosphere-only models. Furthermore, differences in the modeled precipitation responses are consistent with differences in the modelled FWI responses. The primary difference between the models' FWI anthropogenic signals is the northwestern portion of the study area, where CAM5 FWI is increasing and d4PDF-G FWI is unchanged, suggesting there is uncertainty in the FWI anthropogenic response in this region. The divergence appears to be driven by differences in the precipitation and relative humidity responses, as opposed to differences in their temperature responses which are largely increasing across the study area. d4PDF-G precipitation increases in this region with a related increase in relative humidity, while CAM5 does the reverse, each corresponding well to their respective FWI trends. These results suggest that, while global observed extreme fire weather trends have been shown to be largely driven by atmospheric humidity and temperature[9], 6-month averaged FWI behavior at the regional scale may be sensitive to anthropogenic precipitation changes[76].

Natural decadal variability plays a significant role in the observed FWI trends, dampening anthropogenic effects as the natural FWI signal decreases into the 1980s and compounding anthropogenic increases into the 2010s. This multidecadal natural variability pattern is strongest in the southern region of our study area and is consistent with regional effects of the interdecadal pacific oscillation (IPO). Abatzoglou and Williams (2016)[11] suggest observed regional patterns in precipitation over the 1979-2015 period are due to the shifts to the cold phase of the IPO, and contribute to natural increases in fire weather over this period. As such, the commonly used post-1979 and −1984 periods[11,31,39,77,78] are particularly challenging time windows in which to distinguish between the effects of anthropogenic versus natural climate change. In our elongated analyses 1950s-onward analyses, the full cycle of variability is captured in the natural signal making it easily distinguishable from the anthropogenic signal, with the natural response overall contributing decreasing FWI to the observed trends (−31 to −33%). In the commonly-used post-1984 period, however, detection of an anthropogenic fingerprint is less robust (Supplementary Fig 9) and, in the case of d4PDF-G, the natural response is contributing more to the observed increases than the anthropogenic response (~ 26% versus 16%). Detection over this period is still possible, in part due to distinct spatial patterns between the response patterns (Supplementary Fig 13). These results highlight the added value of considering 50+ years of data as well as spatial patterns when studying the effects of anthropogenic climate change on observed fire weather in the presence of large, multi-decadal natural variability.

The atmosphere-only models, d4PDF-G and CAM5, are prescribed different natural SSTs estimations to simulate natural-only forcings scenarios, which may lead to differences in spatial structure between the models, as well as a potential artifact in the case of CAM5. ERA5 FWI trends appear to have spatial structure represented by both models – the latitudinal pattern highlighted by d4PDF-G as well as the coastal and Rocky Mountain influences highlighted by CAM5. While the natural signal is dominated by interannual and decadal variability across the region, the appearance of a linear trend in the NW USA sub-region may be an artifact of an overestimation of the attributable warming in the construction of the naturalized SSTs, at least in the case of CAM5[79]. We tested detectability in the absence of this potential artifact for both models by detrending the natural scenario by local time series means, constructing the new anthropogenic scenario and rerunning the optimal fingerprinting. While this dampened the magnitude of the anthropogenic signal slightly, it did not reduce the detectability of distinct anthropogenic and natural fingerprints.

Our study contains some caveats. The SST-prescribed atmosphere-only modeling experiments imbed any anthropogenic influence on natural ocean variability in the natural scenario, though there is no robust evidence that climate change has affected natural ocean variability, such as the ENSO, at this time scale[69,70]. The resolutions of the CAM5 and d4PDF-G models may be too coarse to accurately simulate local wind gust processes, with wind behavior being inconsistent between the models. Additionally, we

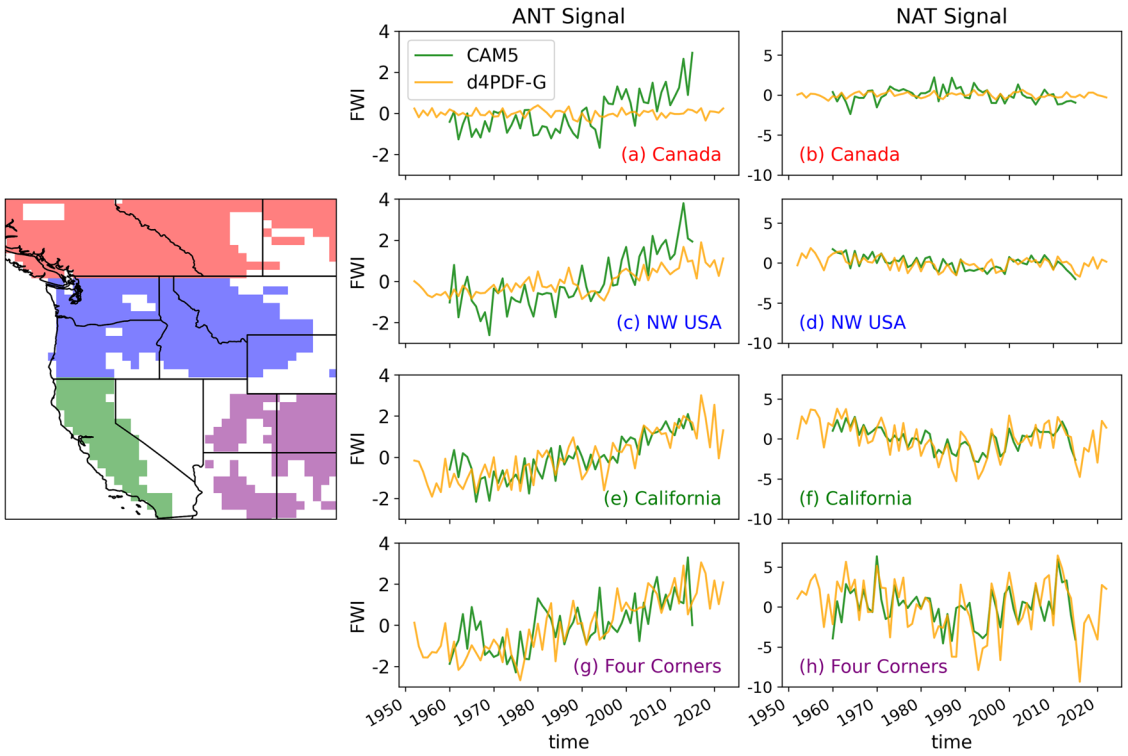

Fig. 5 | Subregional time series of model-simulated signals. Timeseries of ensemble mean anthropogenic (**a**, **c**, **e**, **g**) and natural (**b**, **d**, **f**, **h**) signals for d4PDF-G (1951–2021; orange) and CAM5 (1959–2014; green), grid-cell area weighted averaged within four subregions depicted in the map: Southwest (SW) Canada (**a**, **b**), Northwest (NW) USA (**c**, **d**), California (**e**, **f**), and the Four Corner States (Arizona, Utah, New Mexico, Colorado) (**g**, **h**). Anomalies are taken by removing the time series mean across the entire available time window.

Table 1 | Anthropogenic and natural contributions to observed linear trends

Time Window	Model	Relative Contribution (% of FWI/yr linear trend)					
		ANT			NAT		
		Lower	Best	Upper	Lower	Best	Upper
1951–2021	d4PDF-G	63.19	103.00	142.80	−28.64	−33.26	−37.88
1959–2014	d4PDF-G	47.40	80.77	114.13	−10.96	−12.95	−14.93
	CAM5	159.66	188.45	217.23	−25.93	−30.86	−35.80
1984–2014	d4PDF-G	−1.65	15.72	33.10	22.77	26.17	29.57
	CAM5	65.65	88.23	110.81	9.24	11.29	13.35

Relative contributions (%) of anthropogenic forcings and natural forcings and variability to the observed linear trends in May-October FWI means for selected time windows. Contributions calculated with the best scaling factor estimate are shown alongside contributions calculated with the lower and upper 90th confidence interval scaling factor estimates.

applied a mean-based bias correction for d4PDF-G wind and used daily averages for both models, which removed high wind values which may correspond with higher FWI values[80]. While this bias-correction, and resultant dampening of high daily FWI values had little effect on our 6-month mean fingerprinting analysis (Supplementary Fig 7), it could be problematic for estimating response patterns for extreme FWI values. We have only assessed fire weather D&A using a single fire weather index, though the successful D&A of changes in the underlying meteorological variables – temperature, precipitation, and relative humidity – suggests that the anthropogenic signal is robustly imbedded and that other fire weather indices based on these variables are likely to be detectable as well.

Regional D&A is a historically challenging, low signal-to-noise problem as weak forced signals must be detected in the context of large variability and modelling and observational uncertainties[33,55,59]. Yet, these studies not only improve our physical understanding of how anthropogenic climate change propagates to local-scale processes, but have the potential to provide information to communities and decision makers at the scales that are relevant to them. Here, we detect robust anthropogenic signals at the regional scale with limited reduction of spatial and temporal dimensions. Even in the case of regional temperature D&A, a significant reduction of spatial and temporal dimensions is often required to reliably estimate the covariance matrix of internal variability, i.e. reducing an entire region to a few spatial points or using 5- or 10-year temporal averages[62].

The significance of this study lies in the combined power of optimal fingerprinting and the exceptionally large ensembles of atmosphere-only model simulations produced by d4PDF[71] and C20C + D&A[81]. These large ensembles provide wide samplings of the climate responses and internal variability, strengthening the characterization of both the signals and the noise, and enabling the D&A of regional climate change with limited loss of spatial or temporal information. For example, we use 70 years of daily data from 200 d4PDF-G ensemble members totaling 14000 years of data at 60 km resolution to estimate internal variability. This is an unprecedented sampling in the context other D&A modeling projects, like DAMIP[82], where the typical ensemble sizes range from 1 to 10 members and are not large enough to provide robust estimates of response patterns to external forcings at the regional scale[60,61]. DAMIP models that do provide large ensembles

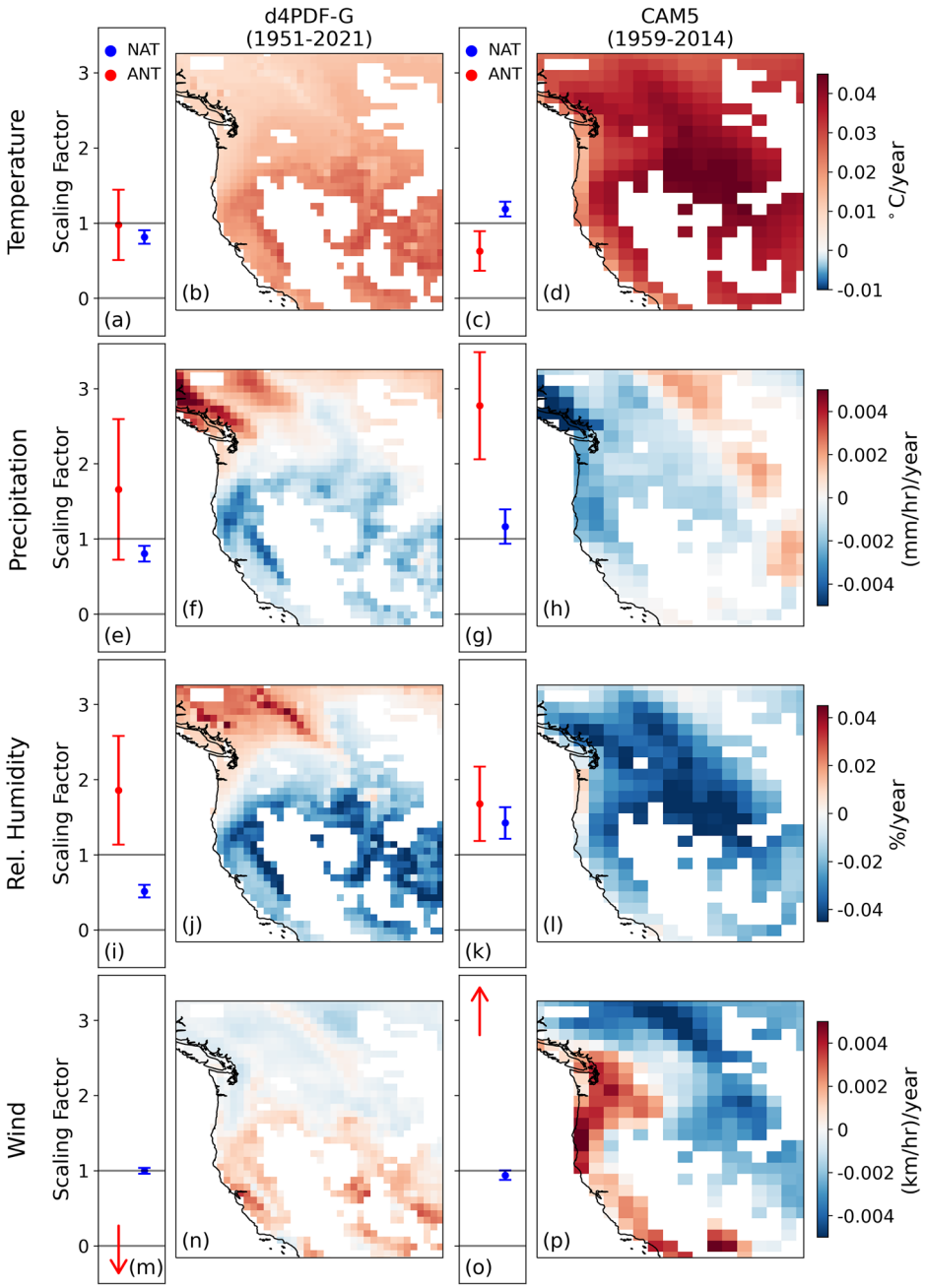

Fig. 6 | Fingerprinting analysis of meteorological variables. Scaling factors and 90% confidence intervals for anthropogenic (red) and natural (blue) response patterns for May-Oct means for the FWI input meteorological variables - temperature (**a**, **b**, **c**, **d**), precipitation (**e**, **f**, **g**, **h**), relative humidity (**i**, **j**, **k**, **l**), and wind (**m**, **n**, **o**, **p**) - alongside a map of the ensemble mean anthropogenic trend (least-square regression slope), for d4PDF-G (1951–2021; **left columns**) and CAM5 (1959–2014; **right columns**). Arrows indicate results are outside the range of the y-axis.

(20+ members) have limited variable availability and low spatial (200 km +) and/or temporal resolutions which limit the use cases of these simulations. The statistical power of these large ensembles not only makes the D&A of regional fire weather a tractable problem, but may enable the detection and attribution of other regions and variables, including extreme values.

The method used in this study could be applied to other regions to explore their unique spatiotemporal anthropogenic and natural fire weather responses, though differences in the strength of signals and size of internal variability will affect detectability in different regions. The application to other regions – or globally – would require the consideration of several factors, including the suitability of the FWI (which is designed for Canadian Boreal forests), the timing and duration of fire seasons, how to mask to areas at risk of fire, and whether to employ overwintering[83]. Further, global application changes the relationship between the dimensions of the signals and the noise. Here, we show that the ensembles provide an adequate sampling of internal variability to detect signals at the regional scale. However, at the global scale, when the spatial dimensions are significantly larger than time, will we need even larger ensembles to adequately characterize the noise?

Data and Methods

Study area

We focus our analysis on a western North America domain west of 104°W, south of 55°N and north of 32°N. Forest types vary across the region, from those dominated by Douglas-firs in the cool, wet regions west of the Cascade mountains, ponderosa-pines in the dryer, high-desert areas, to lodge-pole pine or aspen forests in the cooler northern regions[84]. Wildland fires function as a natural phenomenon in many of these forest ecosystems, and the investigation into historic fire regimes and human-caused changes in this study area has been a prolific topic of recent research[11,84,85]. We limit our analyses to areas with sufficient fuel and thus fire risk by creating a vegetation mask based on a threshold of maximum monthly combined ERA5 high and low vegetation leaf area indices. With a threshold of 3.5, the

vegetation mask excludes plains and deserts and is similar to other forestry-based masks used in other studies[11].

Data sources

We select two atmosphere-only models, d4PDF-G[71] and CAM5[72], to provide anthropogenic and natural response patterns from their d4PDF[86] and C20C + [81] detection and attribution modeling experiments respectively. These models were selected based on having the outputs necessary for calculating FWI, long historical simulations (> 50 years), high resolution (< 100 km), and large ensembles (> 20 members). Each model simulates large ensembles of all-forcing (ALL) and natural-forcing (NAT) detection and attribution scenarios. ALL simulations run with observed trends in greenhouse gases (GHGs), anthropogenic and natural aerosols, and observed variations in sea surface temperatures (SSTs). NAT simulations run with preindustrial GHG and anthropogenic aerosols, and naturalized SSTs. The naturalized SSTs prescribed in the NAT scenarios for each model are estimated by subtracting distinct attributable anthropogenic warming estimates from observed SSTs. For d4PDF-G, the anthropogenic warming signal estimate is the long-term trend of the observed SSTs relative to the 1900–1919 mean[71], while, for CAM5, it is based on the difference between 5-year smoothed monthly CMIP5 historical and natural-forcing only historical simulated skin temperatures[79]. A detailed description of each models' components and physics can be found in Mizuta et al. (2017)[71] and Stone et al. (2018)[72].

Simulated response patterns from these models are compared against FWI calculated from ERA5 reanalysis output in lieu of observations. We use ~110 km CAM5 output from 43 ALL and 49 NAT ensemble members spanning 1959–2014 and ~60 km d4PDF-G output from 100 ensemble members for both ALL and NAT spanning 1951–2021. Some CAM5 ensemble members are not included due to missing data, and data post-2014 is not included due to continuity issues across mid-2015 restarts. We use ERA5 output at 30 km resolution for the years 1951–2021 to calculate FWI. Our ERA5-estimated FWI is coarsened and interpolated to the resolutions of d4PDF-G and CAM5 for their respective optimal fingerprinting analyses. Details on the modeling and observations used in ERA5 can be found in Hersbach et al. (2020)[73].

Fire weather index

The Canadian Fire Weather System (FWI) was designed to provide operational estimates of relative fire potential based on weather station measurements of daily noon dry-bulb temperature, air relative humidity, 10 m wind speed and 24-year accumulated precipitation. Described in detail in van Wagner (1987)[37], the FWI metric is based on a combination of fuel moisture codes that represent daily changes to the moisture context of three classes of forest fuel, as well as indices which represent the rate of spread and fuel weight consumed.

Constraints in model and reanalysis outputs require various levels of deviation from the weather station-based meteorological inputs. Due to the availability of hourly output, ERA5-based FWI calculations are often based on local noon values[83,85,87], while climate-model based calculations are limited to 3-hourly or daily output[36,88,89]. Though there are differences in variable output availability for each data source, we use daily values in each case for consistency, including ERA5. We compared ERA5 FWI calculated with hourly versus daily values and found negligible differences in climatologies and trends. The model variables and calculations used to construct daily FWI inputs for each data source are detailed in Table 2. For d4PDF-G, we used daily maximum temperature, daily mean precipitation, daily minimum relative humidity, and daily mean windspeed to calculate FWI. For CAM5, we use daily maximum temperature, daily mean precipitation, daily mean u/v wind components, and a combination of daily maximum temperature, mean specific humidity, and monthly atmospheric pressure to estimate relative humidity. Daily precipitation accumulation is estimated from daily mean precipitation rates for both models. ERA5 daily FWI inputs are calculated from hourly values, including hourly maximum temperature, hourly accumulated precipitation, hourly mean u/v wind components, and a combination of hourly mean dewpoint temperature and hourly maximum temperature to estimate relative humidity. FWI values were calculated using python code based on the cffdrs R package developed for the Canadian Forest Fire Danger Rating System[90]. Validation analyses of ERA5 FWI against station observations are detailed in Supplementary Note 1.

We average daily FWI values between May and October to construct 6-month mean FWI time series, which are used in the optimal fingerprinting regression analyses, as well as the trend map and time series figures. We use this time window as it encompasses the months when fires are most likely to occur across the entire study area[91], though this is not necessarily the formal fire season for any particular region in the domain. Fire seasons lengths are increasing throughout WNA, with more fires occurring early and late in the season, and for some areas, like California, even outside the time window[85].

Before calculating daily FWI for d4PDF-G, we bias correct d4PDF-G wind to a unimodal distribution. The raw daily windspeed output follows a bimodal distribution with two wind classes separated by orography, perhaps due to how the model simulates the interaction of wind with the model's land surface roughness. See Supplementary Notes 2 and 3 for more details. We test optimal fingerprinting with and without this d4PDF-G wind bias correction (Supplementary Fig 7).

Optimal fingerprinting

Optimal fingerprinting[41,42] is a regression-based D&A method which estimates the relative contributions of anthropogenic and natural response patterns to observed trends by solving the multiple linear regression: $y = X\beta + u$, where y = observations of a real-world system, X = natural and anthropogenic response patterns (signals), β = regression coefficients (scaling factors), and u = residual. Described in detail in Allen and Stott (2003)[92], the regression is performed in the direction of maximum signal-to-noise relative to random variability, which is determined through a weighting of the decomposed empirical orthogonal functions (EOFs) of internal variability. Considering the response patterns in this EOF space, the variability unique to each response pattern relative to noise is isolated and called the 'fingerprint'. The fingerprints are then regressed against the observations in this EOF space to estimate the scaling factors which result in the best linear combination of the response patterns to reproduce the observations. This optimized EOF space can be truncated to exclude some directions of variability, with a tradeoff between not sampling enough variability and overfitting to under sampled, meaningless direction of variability. We perform optimal fingerprinting over all possible truncation levels to assess whether results stabilize.

Two independent estimates of climate 'noise' are required to 1) estimate the covariance matrix used to optimize the regression as described above, and 2) estimate 90% confidence intervals around the scaling factor best estimates. Most optimal fingerprinting studies use fully coupled models to simulate response patterns and construct the independent noise estimates from separate samplings of long preindustrial control simulations. Here, we estimate noise from ALL and NAT ensembles by measuring each member's deviation from the ensemble mean. The independent samples of noise are constructed from the first and second halves of the ALL and NAT noise ensembles respectively.

The range of possible truncation values is dictated by the degrees of freedom for each regression, i.e., the maximum number of independent directions (dimensions) in which one data sample (i.e., observations) can hypothetically be measured to differ from another because of sampling variability (i.e., interval variability). As our estimation of internal variability is constrained by ensemble size (n), we can only hope to measure n different directions. Additionally, the equivalent of two of those dimensions will describe the ALL and NAT responses (even if the 'descriptions' are spread out fractionally across the dimensions) and one will describe the ensemble mean variation, meaning the maximum truncation value is n-3. So, for each regression, possible truncation values range from 3 (# of scenarios + 1) to (n-3). CAM5 has 43 ALL and 49 NAT members (92 total), while d4PDF-G

Table 2 | Climate data used to calculate FWI

Data Source	Temperature	Precipitation	Wind	Relative humidity
ERA5	Daily maximum selected from hourly maximum	Daily accumulation summed from hourly accumulation.	Daily mean wind averaged from hourly wind, which is based on hourly u/v wind components using equation: Wind = 3.6*sqrt(u^2+v^2)	Daily minimum value calculated from the minimum hourly dewpoint temperature and maximum hourly maximum temperature in each day using the MetPy method: relative_humidity_ from_dewpoint.
d4PDF-G	Daily maximum temperature	Daily accumulation estimated from mean daily precipitation rate	Daily mean surface wind speed	Daily minimum relative humidity
CAM5	Daily maximum temperature	Daily accumulation estimated from mean daily precipitation rate	Daily mean wind based on daily u/v wind components using equation: Wind = 3.6*sqrt(u^2+v^2)	Daily minimum relative humidity calculated from daily maximum temperature, daily mean specific humidity and the monthly atmospheric pressure climatology field using MetPy method: relative_humidity _from_specific_humidity

has 100 members for each scenario (200 total). As only half of the ALL and NAT members are used for the internal variability estimation (the other half are used to estimate the confidence intervals), the n in the context above is 100 for d4PDF-G and 46 for CAM5. Thus the range of possible truncations are 3-97 for d4PDF-G and 3-43 for CAM5.

Data availability

d4PDF-G, CAM5 and ERA5 output were downloaded online, from http://search.diasjp.net/search?lang=en&k=d4PDF, https://portal.nersc.gov/c20c/data.html, and https://cds.climate.copernicus.eu/cdsapp#!/dataset/reanalysis-era5-single-levels?tab=overview respectively. Station FWI data was accessed from http://cwfis.cfs.nrcan.gc.ca/downloads/fwi_obs/.

Code availability

The code for the optimal fingerprinting analysis is from the Optimal Detection Package v3.1.3 located here: A Library of IDL Programs. The code used to calculate FWI was adapted from the r-package found here: cffdrs-package: Canadian Forest Fire Danger Rating System in cffdrs: Canadian Forest Fire Danger Rating System.

Received: 23 June 2024; Accepted: 9 May 2025;
Published online: 17 May 2025

References

1. Bowman, D. M. J. S. et al. Vegetation fires in the Anthropocene. *Nat. Rev. Earth Environ.* **1**, 500–515 (2020).
2. Rogers, B. M., Balch, J. K., Goetz, S. J., Lehmann, C. E. R. & Turetsky, M. Focus on changing fire regimes: interactions with climate, ecosystems, and society. *Environ. Res. Lett.* **15**, 030201 (2020).
3. Fusco, E. J., Abatzoglou, J. T., Balch, J. K., Finn, J. T. & Bradley, B. A. Quantifying the human influence on fire ignition across the western USA. *Ecol. Appl.* **26**, 2390–2401 (2016).
4. Keeley, J. E. et al. Ignitions explain more than temperature or precipitation in driving Santa Ana wind fires. *Sci. Adv.* **7**, eabh2262 (2021).
5. Syphard, A. D. & Keeley, J. E. Location, timing and extent of wildfire vary by cause of ignition. *Int. J. Wildland Fire* **24**, 37–47 (2015).
6. Gutierrez, A. A. et al. Wildfire response to changing daily temperature extremes in California's Sierra Nevada. *Sci. Adv.* **7**, eabe6417 (2021).
7. Brown, P. T. et al. Climate warming increases extreme daily wildfire growth risk in California. *Nature* **621**, 760–766 (2023).
8. Ellis, T., Bowman, D., Jain, P., Flannigan, M. & Williamson, G. Global increase in wildfire risk due to climate-driven declines in fuel moisture. *Glob. Change Biol.* **28**, 1544–1559 (2022).
9. Jain, P., Castellanos-Acuna, D., Coogan, S. C. P., Abatzoglou, J. T. & Flannigan, M. D. Observed increases in extreme fire weather driven by atmospheric humidity and temperature. *Nat. Clim. Change* **12**, 63–70 (2022).
10. Jolly, W. M. et al. Climate-induced variations in global wildfire danger from 1979 to 2013. *Nat. Commun.* **6**, 7537 (2015).
11. Abatzoglou, J. T. & Williams, A. P. Impact of anthropogenic climate change on wildfire across western US forests. *Proc. Natl. Acad. Sci.* **113**, 11770–11775 (2016).
12. Abatzoglou, J. T. & Kolden, C. A. Relationships between climate and macroscale area burned in the western United States. *Int. J. Wildland Fire* **22**, 1003–1020 (2013).
13. Littell, J. S., McKenzie, D., Peterson, D. L. & Westerling, A. L. Climate and wildfire area burned in western U.S. ecoprovinces, 1916–2003. *Ecol. Appl.* **19**, 1003–1021 (2009).
14. Williams, A. P. et al. Correlations between components of the water balance and burned area reveal new insights for predicting forest fire area in the southwest United States. *Int. J. Wildland Fire* **24**, 14–26 (2014).
15. Littell, J. S., Peterson, D. L., Riley, K. L., Liu, Y. & Luce, C. H. A review of the relationships between drought and forest fire in the United States. *Glob. Change Biol.* **22**, 2353–2369 (2016).

16. van Oldenborgh, G. J. et al. Pathways and pitfalls in extreme event attribution. *Clim. Change* **166**, 13 (2021).
17. Lewis, S. C. et al. Deconstructing Factors Contributing to the 2018 Fire Weather in Queensland, Australia. *Bull. Am. Meteorol. Soc.* **101**, S115–S122 (2020).
18. Van Oldenborgh, G. J. et al. Attribution of the Australian bushfire risk to anthropogenic climate change. *Nat. Hazards Earth Syst. Sci.* **21**, 941–960 (2021).
19. Krikken, F., Lehner, F., Haustein, K., Drobyshev, I. & Van Oldenborgh, G. J. Attribution of the role of climate change in the forest fires in Sweden 2018. *Nat. Hazards Earth Syst. Sci.* **21**, 2169–2179 (2021).
20. Barbero, R., Abatzoglou, J. T., Pimont, F., Ruffault, J. & Curt, T. Attributing Increases in Fire Weather to Anthropogenic Climate Change Over France. *Front. Earth Sci*. **8**, 104 (2020).
21. Partain, J. L. et al. An Assessment of the Role of Anthropogenic Climate Change in the Alaska Fire Season of 2015. *Bull. Am. Meteorol. Soc.* **97**, S14–S18 (2016).
22. Tan, X., Chen, S. & Gan, T. Y. Multi-model extreme event attribution of the weather conducive to the 2016 Fort McMurray wildfire. *Agric. For. Meteorol.* **260–261**, 109–117 (2018).
23. Hawkins, L. R., Abatzoglou, J. T., Li, S. & Rupp, D. E. Anthropogenic Influence on Recent Severe Autumn Fire Weather in the West Coast of the United States. *Geophys. Res. Lett.* **49**, e2021GL095496 (2022).
24. Kirchmeier-Young, M. C., Zwiers, F. W., Gillett, N. P. & Cannon, A. J. Attributing extreme fire risk in Western Canada to human emissions. *Clim. Change* **144**, 365–379 (2017).
25. Kirchmeier-Young, M. C., Gillett, N. P., Zwiers, F. W., Cannon, A. J. & Anslow, F. S. Attribution of the Influence of Human-Induced Climate Change on an Extreme Fire Season. *Earths Future* **7**, 2–10 (2019).
26. Kirchmeier-Young, M. C. et al. Human driven climate change increased the likelihood of the 2023 record area burned in Canada. *Npj Clim. Atmospheric Sci.* **7**, 1–12 (2024).
27. Liu, Z., Eden, J. M., Dieppois, B. & Blackett, M. A global view of observed changes in fire weather extremes: uncertainties and attribution to climate change. *Clim. Change* **173**, 14 (2022).
28. Touma, D., Stevenson, S., Lehner, F. & Coats, S. Human-driven greenhouse gas and aerosol emissions cause distinct regional impacts on extreme fire weather. *Nat. Commun.* **12**, 212 (2021).
29. Gillett, N. P., Weaver, A. J., Zwiers, F. W. & Flannigan, M. D. Detecting the effect of climate change on Canadian forest fires. *Geophys. Res. Lett*. **31**, L18211 (2004).
30. Turco, M. et al. Anthropogenic climate change impacts exacerbate summer forest fires in California. *Proc. Natl. Acad. Sci.* **120**, e2213815120 (2023).
31. Zhuang, Y., Fu, R., Santer, B. D., Dickinson, R. E. & Hall, A. Quantifying contributions of natural variability and anthropogenic forcings on increased fire weather risk over the western United States. *Proc. Natl. Acad. Sci.* **118**, e2111875118 (2021).
32. Kirchmeier-Young, M. C. & Zhang, X. Human influence has intensified extreme precipitation in North America. *Proc. Natl. Acad. Sci.* **117**, 13308–13313 (2020).
33. Sarojini, B., Stott, P. & Black, E. Detection and attribution of human influence on regional precipitation. *Nat. Clim. Change* **6**, 669–675 (2016).
34. Risser, M. D. et al. A framework for detection and attribution of regional precipitation change: Application to the United States historical record. *Clim. Dyn.* **60**, 705–741 (2023).
35. Flannigan, M. D. et al. Fuel moisture sensitivity to temperature and precipitation: climate change implications. *Clim. Change* **134**, 59–71 (2016).
36. Abatzoglou, J. T., Williams, A. P. & Barbero, R. Global Emergence of Anthropogenic Climate Change in Fire Weather Indices. *Geophys. Res. Lett.* **46**, 326–336 (2019).
37. Van Wagner, C. E. Development and Structure of the Canadian Forest Fire Weather Index System. *Can. For. Serv*. Forestry Technical Report **35**, 35 p (1987).
38. Abatzoglou, J. T., Williams, A. P., Boschetti, L., Zubkova, M. & Kolden, C. A. Global patterns of interannual climate-fire relationships. *Glob. Change Biol.* **24**, 5164–5175 (2018).
39. Jones, M. W. et al. Global and Regional Trends and Drivers of Fire Under Climate Change. *Rev. Geophys.* **60**, e2020RG000726 (2022).
40. Gincheva, A. et al. The Interannual Variability of Global Burned Area Is Mostly Explained by Climatic Drivers. *Earths Future* **12**, e2023EF004334 (2024).
41. Allen, M. R. & Tett, S. F. B. Checking for model consistency in optimal fingerprinting. *Clim. Dyn.* **15**, 419–434 (1999).
42. Hasselmann, K. Optimal Fingerprints for the Detection of Time-dependent Climate Change. *J. Clim.* **6**, 1957–1971 (1993).
43. Hegerl, G. C. et al. Multi-fingerprint detection and attribution analysis of greenhouse gas, greenhouse gas-plus-aerosol and solar forced climate change. *Clim. Dyn.* **13**, 613–634 (1997).
44. Stott, P. A. et al. Attribution of twentieth century temperature change to natural and anthropogenic causes. *Clim. Dyn.* **17**, 1–21 (2001).
45. Santer, B. D. et al. Behavior of tropopause height and atmospheric temperature in models, reanalyses, and observations: Decadal changes. *J. Geophys. Res. Atmospheres* **108**, ACL 1-1-ACL 1-22 (2003).
46. Tebaldi, C., Hayhoe, K., Arblaster, J. M. & Meehl, G. A. Going to the Extremes. *Clim. Change* **79**, 185–211 (2006).
47. Jones, G. S., Stott, P. A. & Christidis, N. Attribution of observed historical near–surface temperature variations to anthropogenic and natural causes using CMIP5 simulations. *J. Geophys. Res. Atmospheres* **118**, 4001–4024 (2013).
48. Lambert, F. H., Gillett, N. P., Stone, D. A. & Huntingford, C. Attribution studies of observed land precipitation changes with nine coupled models. *Geophys. Res. Lett*. **32**, L18704 (2005).
49. Zhang, X., Wan, H., Zwiers, F. W., Hegerl, G. C. & Min, S.-K. Attributing intensification of precipitation extremes to human influence. *Geophys. Res. Lett.* **40**, 5252–5257 (2013).
50. Willett, K. M., Gillett, N. P., Jones, P. D. & Thorne, P. W. Attribution of observed surface humidity changes to human influence. *Nature* **449**, 710–712 (2007).
51. Barnett, T. P. et al. Penetration of Human-Induced Warming into the World's Oceans. *Science* **309**, 284–287 (2005).
52. Gudmundsson, L. et al. Globally observed trends in mean and extreme river flow attributed to climate change. *Science* **371**, 1159–1162 (2021).
53. Zhou, T. & Zhang, W. Anthropogenic warming of Tibetan Plateau and constrained future projection. *Environ. Res. Lett.* **16**, 044039 (2021).
54. Xu, Y., Gao, X., Shi, Y. & Zhou, B. Detection and attribution analysis of annual mean temperature changes in China. *Clim. Res*. **63**, 61–71 (2015).
55. Li, C., Zhao, T. & Ying, K. Quantifying the contributions of anthropogenic and natural forcings to climate changes over arid-semiarid areas during 1946–2005. *Clim. Change* **144**, 505–517 (2017).
56. Dileepkumar, R., AchutaRao, K. & Arulalan, T. Human influence on sub-regional surface air temperature change over India. *Sci. Rep.* **8**, 8967 (2018).
57. Peng, D., Zhou, T., Zhang, L. & Zou, L. Detecting human influence on the temperature changes in Central Asia. *Clim. Dyn.* **53**, 4553–4568 (2019).
58. Wan, H., Zhang, X. & Zwiers, F. Human influence on Canadian temperatures. *Clim. Dyn.* **52**, 479–494 (2019).
59. Wan, H., Zhang, X., Zwiers, F. & Min, S.-K. Attributing northern high-latitude precipitation change over the period 1966–2005 to human influence. *Clim. Dyn.* **45**, 1713–1726 (2015).
60. Maher, N. et al. The Max Planck Institute Grand Ensemble: Enabling the Exploration of Climate System Variability. *J. Adv. Model. Earth Syst.* **11**, 2050–2069 (2019).
61. Deser, C. et al. Insights from Earth system model initial-condition large ensembles and future prospects. *Nat. Clim. Change* **10**, 277–286 (2020).

62. Doblas-Reyes, F. J. et al. Linking global to regional climate change. in *Climate Change 2021: The Physical Science Basis. Contribution of Working Group I to the Sixth Assessment Report of the Intergovernmental Panel on Climate Change* (eds. Masson-Delmotte, V. et al.) 1363–1512 (Cambridge University Press, Cambridge, United Kingdom and New York, NY, USA, 2021). https://doi.org/10.1017/9781009157896.001.
63. Najafi, M. R., Zwiers, F. W. & Gillett, N. P. Attribution of Arctic temperature change to greenhouse-gas and aerosol influences. *Nat. Clim. Change* **5**, 246–249 (2015).
64. Gillett, N. P. et al. Constraining human contributions to observed warming since the pre-industrial period. *Nat. Clim. Change* **11**, 207–212 (2021).
65. Hu, T., Sun, Y., Zhang, X., Min, S.-K. & Kim, Y.-H. Human influence on frequency of temperature extremes. *Environ. Res. Lett.* **15**, 064014 (2020).
66. Paik, S. et al. Determining the Anthropogenic Greenhouse Gas Contribution to the Observed Intensification of Extreme Precipitation. *Geophys. Res. Lett.* **47**, e2019GL086875 (2020).
67. Kay, J. E. et al. The Community Earth System Model (CESM) Large Ensemble Project: A Community Resource for Studying Climate Change in the Presence of Internal Climate Variability. *Bull. Am. Meteorol. Soc.* **96**, 1333–1349 (2015).
68. He, J. & Soden, B. J. The impact of SST biases on projections of anthropogenic climate change: A greater role for atmosphere-only models?. *Geophys. Res. Lett.* **43**, 7745–7750 (2016).
69. Planton, Y. Y. et al. Evaluating Climate Models with the CLIVAR 2020 ENSO Metrics Package. *Bull. Am. Meteorol. Soc.* **102**, E193–E217 (2021).
70. Stevenson, S., Capotondi, A., Fasullo, J. & Otto-Bliesner, B. Forced changes to twentieth century ENSO diversity in a last Millennium context. *Clim. Dyn.* **52**, 7359–7374 (2019).
71. Mizuta, R. et al. Over 5,000 Years of Ensemble Future Climate Simulations by 60-km Global and 20-km Regional Atmospheric Models. *Bull. Am. Meteorol. Soc.* **98**, 1383–1398 (2017).
72. Stone, D. A. et al. A basis set for exploration of sensitivity to prescribed ocean conditions for estimating human contributions to extreme weather in CAM5.1-1degree. *Weather Clim. Extrem.* **19**, 10–19 (2018).
73. Hersbach, H. et al. The ERA5 global reanalysis. *Q. J. R. Meteorol. Soc.* **146**, 1999–2049 (2020).
74. Ribes, A., Planton, S. & Terray, L. Application of regularised optimal fingerprinting to attribution. Part I: method, properties and idealised analysis. *Clim. Dyn.* **41**, 2817–2836 (2013).
75. Parisien, M.-A. et al. Abrupt, climate-induced increase in wildfires in British Columbia since the mid-2000s. *Commun. Earth Environ.* **4**, 1–11 (2023).
76. Holden, Z. A. et al. Decreasing fire season precipitation increased recent western US forest wildfire activity. *Proc. Natl. Acad. Sci.* **115**, E8349–E8357 (2018).
77. Singleton, M. P., Thode, A. E., Sánchez, Meador, A. J. & Iniguez, J. M. Increasing trends in high-severity fire in the southwestern USA from 1984 to 2015. *For. Ecol. Manag.* **433**, 709–719 (2019).
78. Parks, S. A. & Abatzoglou, J. T. Warmer and Drier Fire Seasons Contribute to Increases in Area Burned at High Severity in Western US Forests From 1985 to 2017. *Geophys. Res. Lett.* **47**, e2020GL089858 (2020).
79. Stone, D. A. & Pall, P. Benchmark estimate of the effect of anthropogenic emissions on the ocean surface. *Int. J. Climatol.* **41**, 3010–3026 (2021).
80. Dowdy, A. J., Mills, G. A., Finkele, K. & de Groot, W. Index sensitivity analysis applied to the Canadian Forest Fire Weather Index and the McArthur Forest Fire Danger Index. *Meteorol. Appl.* **17**, 298–312 (2010).
81. Stone, D. A. et al. Experiment design of the International CLIVAR C20C + Detection and Attribution project. *Weather Clim. Extrem.* **24**, 100206 (2019).
82. Gillett, N. P. et al. The Detection and Attribution Model Intercomparison Project (DAMIP v1.0) contribution to CMIP6. *Geosci. Model Dev.* **9**, 3685–3697 (2016).
83. McElhinny, M., Beckers, J. F., Hanes, C., Flannigan, M. & Jain, P. A high-resolution reanalysis of global fire weather from 1979 to 2018 – overwintering the Drought Code. *Earth Syst. Sci. Data* **12**, 1823–1833 (2020).
84. Hagmann, R. K. et al. Evidence for widespread changes in the structure, composition, and fire regimes of western North American forests. *Ecol. Appl.* **31**, e02431 (2021).
85. Jain, P., Wang, X. & Flannigan, M. D. Trend analysis of fire season length and extreme fire weather in North America between 1979 and 2015. *Int. J. Wildland Fire* **26**, 1009–1020 (2017).
86. Ishii, M. & Mori, N. d4PDF: large-ensemble and high-resolution climate simulations for global warming risk assessment. *Prog. Earth Planet. Sci.* **7**, 58 (2020).
87. Vitolo, C., Di Giuseppe, F., Krzeminski, B. & San-Miguel-Ayanz, J. A. 1980–2018 global fire danger re-analysis dataset for the Canadian Fire Weather Indices. *Sci. Data* **6**, 190032 (2019).
88. Quilcaille, Y., Batibeniz, F., Ribeiro, A. F. S., Padrón, R. S. & Seneviratne, S. I. Fire weather index data under historical and shared socioeconomic pathway projections in the 6th phase of the Coupled Model Intercomparison Project from 1850 to 2100. *Earth Syst. Sci. Data* **15**, 2153–2177 (2023).
89. Jain, P., Tye, M. R., Paimazumder, D. & Flannigan, M. Downscaling fire weather extremes from historical and projected climate models. *Clim. Change* **163**, 189–216 (2020).
90. Wang, X. et al. An R package for the Canadian Forest Fire Danger Rating System. *Ecol. Process*. **6**, 5 (2017).
91. Westerling, A. L., Gershunov, A., Brown, T. J., Cayan, D. R. & Dettinger, M. D. Climate and Wildfire in the Western United States. *Bull. Am. Meteorol. Soc.* **84**, 595–604 (2003).
92. Allen, M. R. & Stott, P. A. Estimating signal amplitudes in optimal fingerprinting, part I: theory. *Clim. Dyn.* **21**, 477–491 (2003).

Author contributions

L.Q. performed the analyses and lead the writing of the manuscript. S.D., D.S. and J.R. advised on the direction of the research and the construction of the manuscript. P.J. and N.M. contributed expertise and their revisions to the manuscript. Y.I. contributed data for analysis.

Competing interests

The authors declare no competing interests.

Additional information

Supplementary information The online version contains supplementary material available at https://doi.org/10.1038/s43247-025-02372-4.

Correspondence and requests for materials should be addressed to Laura E. Queen.

Peer review information *Communications Earth & Environment* thanks and the other, anonymous, reviewer(s) for their contribution to the peer review of this work. Primary Handling Editor: Alireza Bahadori. A peer review file is available.